

Optical studies of ultra-luminous X-ray sources in nearby galaxies

Ji-Feng Liu, Joel N. Bregman, Patrick Seitzer, and Jimmy Irwin

Astronomy Department, University of Michigan, MI 48109

ABSTRACT

Optical studies of ultra-luminous X-ray sources is an essential step in understanding the nature of these enigmatic sources, and in this paper we report our studies of five ULXs in NGC4559, NGC5194, NGC1313 and NGC628 observed with the Hubble Space Telescope and the 6.4 Magellan/Baade telescope. The ULX in NGC4559 is identified with four blue and red supergiants within a $0''.2$ error circle, in a star forming region that is younger than $10^{7.4}$ years. ULX-3 in NGC5194 is located on the rim of a star cluster with a few faint stars within the $0''.3$ error circle, though the secondary in this system is expected to be a low mass ($0.3M_{\odot}$) star below detection limits given its two hour period. ULX-5 in NGC5194 is located on a spiral arm with seven objects within the $0''.8$ error circle, which can be improved with future observations. Both ULXs in NGC5194 are in regions younger than $10^{7.8}$ years. The ULXs in NGC1313 and NGC628 was observed with the Baade telescope. The ULX in NGC1313 is identified with one object with R-I color bluer than the bluest stellar objects, indicative of non-thermal emission in the R band, or dramatic variability between two observations, or errors in measurements. The ULX in NGC628 is located in a bubble nebula and identified with a few extended objects that are probably young stellar clusters. Future observations with better spatial resolutions are needed to clarify the optical counterparts and their nature for the ULXs in NGC1313 and NGC628.

Subject headings: X-rays: binaries – X-rays: galaxies – Optical: binaries

1. INTRODUCTION

Ultra-luminous X-ray sources (ULXs) are extra-nuclear sources with luminosities in the range of $10^{39} - 10^{41}$ erg/sec in other galaxies, and have been observed by Einstein (e.g., Fabiano et al. 1989), ROSAT (e.g., Colbert 1999), ASCA (e.g., Makishima et al.

2001), recently by XMM-Newton and Chandra Observatory in many galaxies (e.g., Kilgard et al. 2002; Swartz et al. 2004). As compared to the cases of the X-ray binaries in our Galaxy, which are powered by accretion onto neutron stars or stellar mass black holes and have luminosities of $10^{33} - 10^{38}$ erg/sec, the luminosities of ULXs require accreting black holes of masses $10^3 - 10^4 M_{\odot}$ if they emit at 10^{-2} of the Eddington luminosity, typical of Galactic X-ray binaries. Such intermediate mass black holes (IMBHs), if they exist, bridge up the gap between stellar mass black holes and supermassive black holes of $10^6 - 10^9 M_{\odot}$ in the center of galaxies. However, such IMBHs are not predicted to be the products of ordinary stellar evolution models, and it is still in debate whether they can form in dense stellar fields via runaway stellar collisions with seed BHs of a few hundred M_{\odot} (e.g., Portegies Zwart 2002). Alternatively, these sources can be stellar mass black holes, for which the formation is well established in theory and observation. Special mechanisms are required for these stellar mass black holes to emit at super-Eddington luminosities. Such a mechanism could be extreme relativistic beaming (Georganopoulos et al. 2002), mild geometric beaming (e.g., King et al. 2001; Abramowics et al. 1978), or the photon-bubble instability in a radiation pressure dominated accretion disk, which leads to truly super-Eddington luminosities (Begelman 2002).

The ultimate goal in ULX studies is to determine the mass of the primary of ULX systems. While the primary mass can be estimated through the X-ray spectra (e.g. Miller et al. 2003) or possible quasi-periodic oscillations (e.g. Strohmayer et al. 2003), the oldest yet most secure way is to measure the mass function through the secondary mass and the orbital parameters such as the velocities, the period, and/or the orbit size, which could be done through spectroscopic observations of the optical secondary. The first step of this method is to identify the secondary in optical, which is challenging because ULXs are usually located in star forming regions where star density is very high and there could be a few tens of objects even within a small error circle of $1''$ radius. To identify a ULX to one unique counterpart, one needs its X-ray position accurate to a few tenth of arcseconds. Such positional accuracy can only be obtained with Chandra observations, which have uncertainties of $\sim 0''.6$, and can be further improved with relative astrometry. One also needs to be able to resolve the bright objects in the error circle, which can be done for star forming regions only in nearby galaxies given the limitation on the spatial resolution of the telescopes of our time.

Optical studies of ULXs and their environments have been carried out with both large ground-based telescopes and the Hubble Space Telescope. Pakull & Mirioni (2002) surveyed fifteen ULXs in eleven nearby galaxies with ground based telescopes, and found HII regions, (bubble) nebulae, and X-ray ionized nebulae (XIN) within the error circles of their ROSAT HRI positions. Kaaret et al. (2004) observed the XIN at the location of the ULX in Holmberg II with HST/ACS, and found a bright, point-like counterpart for which the magnitude and

color are consistent with a star between O4V and B3 Ib, or reprocessed emission from an X-ray illuminated accretion disk. Zampieri et al. (2004) found for the ULX in NGC1313 a faint optical counterpart within the surrounding bubble nebula with ESO 3.6m telescope. Cropper et al. (2004) found multiple objects on HST/WFPC2 images within the $0''.7$ error circle around the nominal Chandra position for the ULX in NGC4559.

We have studied a sample of ULXs in nearby galaxies with HST and the Magellan/Baade 6.4-meter telescope. This has led to the successful identifications of the ULX in NGC3031 (Liu et al. 2002) and the ULX in NGC5204 (Liu et al. 2004). The ULX in NGC3031 is identified to a unique point-like object on the WFPC2 images, for which the magnitudes and colors are consistent with those for an O8V star that is presumably the optical secondary in the ULX system. Unlike the high-mass X-ray binary (HMXB) systems in our Galaxy that are accreting mass through stellar wind, the O8V star in this system may be filling its Roche Lobe and accreting mass onto the primary with much higher accretion efficiency that leads to its high X-ray luminosity. For the ULX in NGC5204, we have found a unique optical counterpart with the HST ACS/HRC images and, from its HST STIS spectrum, determined the secondary to be a B0 Ib supergiant which is presumably overflowing its Roche Lobe and accreting materials onto the primary black hole. There is a NV emission line at 1240\AA in its spectrum suggestive of an accretion disk, since the high ionization state of NV cannot occur in a B0 Ib star, but is easily achievable in an accretion disk and its corona as observed in some low mass X-ray binaries (LMXBs) such as LMC X-3 and Hercules X-1.

In this paper we report our results on the rest ULXs in our sample. Among these, one ULX in NGC4559 is identified to four neighboring objects in HST/WFPC2 images with much improved astrometry, two ULXs on the spiral arms in NGC5194 show multiple objects in the error circles of Chandra positions, with one ULX located on the rim of a star forming knot. The ULXs in NGC1313 and NGC628 studied with the Baade telescope are also reported here.

2. DATA ANALYSIS AND RESULTS

Optical studies of ULXs in star forming regions require the combination of very accurate X-ray and optical positions and high spatial resolution of the optical images. For accurate X-ray positions, we utilize the Chandra ACIS observations, which have a typical accuracy of $0''.6$ for absolute positions (Aldcroft et al. 2000). The ACIS data were analyzed with CIAO 2.3 and CALDB 2.12, and WAVDETECT was run to detect discrete sources on ACIS-S chips. The X-ray luminosities for ULXs were estimated from their count rates by assuming a power-law spectrum in 0.3–8 KeV with a photon index of 1.7, consistent with the average

photon index for ULXs in nearby galaxies (Swartz et al. 2004).

The Hubble Space Telescope provides the best spatial resolution for optical observations. HST images in three filters of F450W (B), F555W (V) and F814W (I) were taken for a sample of ULXs in nearby galaxies for our HST program (GO 9073) with the Wide Field and Planetary Camera (WFPC2). The pixel size for the Planetary Camera chip is $0''.05$, and $0''.1$ for the three Wide Field chips. We used HSTphot (Dolphin 2000) to perform PSF fitting photometry. The absolute accuracy of the positions obtained from WFPC2 images is typically $0''.5$ R.M.S. in each coordinate (HST data handbook). The relative positions have higher accuracy, which is better than $0''.005$ for targets contained on one chip, and $0''.1$ for targets on different chips.

A direct overlay of the X-ray position on the HST WFPC2 image would yield an error circle of $0''.8$, unable to identify the ULX with a unique object in dense stellar fields. However, the error circle can be greatly reduced when one or more nearby X-ray sources are identified with objects on the same optical image, so that the ULX can be registered on the optical image relative to the counterparts for the nearby X-ray sources. This technique of relative astrometry involves the accuracies of relative positions for objects on the X-ray and optical images which are better than the accuracies of absolute positions, and usually leads to error circles of a few tenths of arcseconds, small enough to enclose only one object in moderately dense stellar fields. This technique has been successfully applied for the ULXs in NGC3031 and NGC5204, each of which is identified with a unique point-like object within the much reduced error circle ($\sim 0''.2$). The technique is also used to improve the positional accuracies on the optical images for the ULXs reported in this paper.

While limited by the seeing, the observations with large ground based telescopes still play a role in identifying the optical counterparts for ULXs, especially for those in less dense stellar fields. We observed a sample of ULXs in nearby galaxies with the Inamori Magellan Areal Camera and Spectrograph (IMACS) mounted on the 6.4-meter Magellan/Baade telescope in November 2003, and achieved a seeing of $\sim 0''.6$. The IMACS images of 2X4 mosaic CCDs have a $15' \times 15'$ field of view with a pixel scale of $0''.11/\text{pixel}$. The large field of view of the IMACS images is advantageous to relative astrometry, since more X-ray sources with optical counterparts would be found near the ULX in a larger image. This expectation is verified in the case of the ULX in NGC628. The photometry of our observations is calibrated with short exposures of the photometric standard field L98¹.

In the following, we report the observations and analysis on the five ULXs in NGC4559, NGC5194, NGC1313 and NGC628.

¹<http://cadwww.dao.nrc.ca/cadcbn/wdb/astrocat/stetson/query/L98>

2.1. A ULX in NGC4559

NGC4559 is a Scd spiral galaxy with a distance reported from 9.7 Mpc (Tully 1988) to 5.8 Mpc (Tully 1992). X-ray observations with ROSAT, XMM, and Chandra observatories have revealed two ULXs in the galaxy. One ULX is close to but not the nucleus, another is 2' south of the nucleus and located on an outer spiral arm. Here we study the latter.

This ULX have been observed with Chandra three times in January 2001 (Observation ID 2026, 9 kiloseconds), June 2001 (ObsID 2027, 10 kiloseconds), and March 2002 (ObsID 2686, 3 kiloseconds). The average position for the ULX from three Chandra observations is R.A.=13h35m51.7s, Decl.=27d56m04.7s. Placed at a distance of 5.8 (9.7) Mpc, the ULX shows an X-ray luminosity of 9.2×10^{39} (2.6×10^{40}) erg/sec in June 2001, making it one of the most extreme ULXs. Its luminosity dropped to 4.8×10^{39} (1.3×10^{40}) erg/sec in March 2002, exhibiting a dramatic drop of 50% in nine months. Cropper et al. (2004) studied the spectra in Chandra observations and in an XMM observation, and found that all spectra show a soft component that can be fitted with a disk temperature of ~ 0.12 KeV, suggestive of a black hole of $M_{\bullet} \geq 10^3 M_{\odot}$ if interpreted as the inner disk temperature of the accretion disk around the black hole. For timing analysis, they computed the power density spectrum for the ULX, and found a break in the power-law fit at $f_b = 28$ mHz, which indicates the black hole mass $M_{\bullet} = 40$ (1300) M_{\odot} if f_b is taken as the lower (higher) low frequency break in the M_{\bullet} - f_b scaling relation as demonstrated in AGNs and X-ray binaries such as Cygnus X-1 (Belloni & Hasinger 1990).

The ULX has been observed with HST/WFPC2 in filters F450W (B), F555W (V) and F814W (I). A direct comparison of the X-ray images with the WFPC2 images yields five bright objects and many more faint objects within the 0'7 error circle around the nominal Chandra position of the ULX (Cropper et al. 2004). Fortunately, relative astrometry can be done to improve the positional accuracy due to two nearby X-ray sources (X4 and X5) that show optical counterparts on the WFPC2 images. The ULX and X4 were detected in the second observation. X4 falls on the WF2 chip, and is identified with an extended object that is an elliptical galaxy or an edge-on spiral galaxy in the background. The ULX and X5 were detected in the third observation. X5 falls on the WF3 chip, and is identified with a bright point-like object that may be a foreground star. The X-ray positions and optical positions for X4 and X5, and derived optical positions for the ULX are listed in Table 1. The error circles around the corrected ULX positions derived from X4 and X5 have radii of $\sim 0'3$, and are plotted in Figure 1. The two error circles partly overlap each other, and in the overlapping region is one point-like object. Another three point-like objects are within the error circle derived from X5. In total, four point-like objects are identified as candidates for the optical counterpart of the ULX, and the rest in the 0'7 nominal error circle adopted by

Cropper et al. (2004) are excluded. The magnitudes for the four candidates are calculated with HSTphot and listed in Table 2.

The four candidates form a close association, and lie between two young star clusters in a star forming complex on the outer edge of NGC4559. The star forming complex is isolated from other star forming regions/knots on the inner spiral arms, and is probably triggered by a recent plunge of a nearby dwarf galaxy through the disk (Soria et al. 2004). The bright stars form two distinct groups on the color-magnitude diagram, one of blue OB stars, and one of red supergiants (Figure 2). The ages can be estimated by comparing the colors and magnitudes of the stars to isochrones, for which we use the isochrones from the Geneva stellar models (Lejeune & Schaerer 2001) with $Z=0.020$ given the low metal abundance of the environments (Soria et al. 2004). As seen from Figure 2, the red supergiants span the age range of $10^{7.4}$ – $10^{7.6}$ ($10^{7.2}$ – $10^{7.4}$) years if a distance of 5.8 (9.7) Mpc is adopted. This is consistent with the age estimate of ≤ 30 Myrs by Soria et al. using a distance of 9.7 Mpc (2004). The bright blue stars are younger than $10^{7.2}$ (10^7) years. For the faint stars, the large errors in their colors prevents an estimate of the ages. Among the four candidates, three less brighter candidates are evolved red supergiants in the age range of 25–40 (15–25) Myrs, while the brightest one is a blue star/supergiant that is leaving the main sequence, with an age of ≤ 15 (≤ 10) Myrs.

The spectral type and luminosity class, thus the mass and size of a stellar object can be inferred from comparing its absolute magnitudes and colors to those of different MK types. Here the extinction is corrected for the Galactic HI column density of $1.5 \times 10^{20} \text{ cm}^{-2}$, which corresponds to $A_B=0.106$ mag, $A_V=0.080$ mag, and $A_I=0.049$ mag if we adopt the relation $n_H = 5.8 \times 10^{21} \times E(B - V)$ (Bohlin, Savage, & Drake 1978) and $R_V = 3.1$. The extinction intrinsic to NGC4559, though may be larger than the Galactic extinction, is neglected since they must be small with $E(B - V) < 0.1$ mag, or else the blue OB population would be significantly bluer than stellar models can predict as seen in Figure 2. The color $B - V$ and the absolute magnitude M_V for the four candidates (Table 2) are compared to those of different MK types as tabulated in Schmidt-Kaler (1982). If we adopt a distance of 5.8 Mpc ($\mu=28.82$ mag), the candidate C-1 is consistent with a B2 Ib supergiant ($M_V=-5.7$, $B - V=-0.18$), C-2 is consistent with an F8 Ib supergiant ($M_V=-5.1$, $B - V=0.56$), C-3 is consistent with a G5 Ib supergiant ($M_V=-4.6$, $B - V=1.00$), and C-4 lies between F2 Ib ($M_V=-5.1$, $B - V=0.23$) and F2 II ($M_V=-2.4$, $B - V=0.30$).

The candidates will be identified to different MK types if we adopt a different distance thus different absolute magnitudes for the candidates. For a distance of 9.7 Mpc ($\mu=29.93$ mag), C-1 is most consistent with a B1 Ia supergiant ($M_V=-6.9$, $B - V=-0.19$). For C-2, its color is consistent with an F8 Ib or F8 Iab supergiant ($M_V=-6.5$, $B - V=0.56$), while its

M_V is brighter than F8 Ib by 0.9 mag, and dimmer than F8 Iab by 0.5 mag. For C-3, its color is consistent with a G5 Ib or G5 Iab ($M_V=-6.2$, $B - V=1.02$) supergiant, while its M_V is brighter than G5 Ib by 0.5 mag, and dimmer than G5 Iab by 0.6 mag. For C-4, the color lie between an F2 Ib supergiant and an F5 Ib supergiant ($M_V=-5.1$, $B - V=0.33$), while it is brighter than such supergiants by 0.2 mag.

The above inferred spectral types are subject to errors due to uncertainties of the distance and the intrinsic extinction. For example, if the total extinction amounts to $E(B - V)=0.1$ mag (thus $A_B=0.408$ mag and $A_V=0.308$ mag for $R_V=3.1$), C-1 would have $M_V=-5.97$ and $B - V=-0.26$ at a distance of 5.8 Mpc, consistent with a supergiant between B0 Ib ($M_V=-6.1$, $B - V=-0.24$) and B0 II ($M_V=-5.7$, $B - V=-0.29$). A more robust way to classify the candidates to MK spectral types is to take spectra with low or medium resolutions that can reveal the spectral shape and even line features. The mass and size of the stars can be inferred empirically once the spectral types are known, and the mass of the primary can be calculated if one star is identified as the secondary with improved astrometry and the orbital velocities is known with further spectroscopic observations.

2.2. Two ULXs in NGC5194

NGC5194 (M51) is a grand-design Sbc galaxy at a distance of 7.7 Mpc (Tully 1988) which is interacting with its companion NGC5195. Six ULXs have been discovered in M51 with ROSAT HRI observations (Liu & Bregman 2005), greatly exceeding the average of 0.72 ± 0.11 ULXs per spiral galaxy as discovered in a recent HRI survey of ULXs in nearby galaxies (Liu, Bregman & Irwin, 2004). All ULXs are located on the spiral arms, and here we study two of them, the ULX-3 and ULX-5 as designated in Liu & Bregman (2005).

ULX-3 has been observed with Chandra three times in January 2000 (ObsID 414, 1 kilosecond), June 2000 (ObsID 354, 15 kiloseconds), and in June 2001 (ObsID 1622, 27 kiloseconds). The average X-ray position for ULX-3 from the last two observations is R.A.=13h30m01.0s, Decl.=47d13m44.0s. Some interesting properties for this ULX has been revealed from the Chandra observations (Liu et al. 2002). In one year between the last two observations, the luminosity dropped dramatically from $\sim 2 \times 10^{39}$ erg/sec to $\sim 8 \times 10^{37}$ erg/sec, 4% of the original level. Along with the dramatic luminosity decrease, the X-ray spectra changed from a hard/high state to a soft/low state, in contradiction to the soft/high to hard/low transition commonly seen in Galactic LMXBs. Most remarkably, a two hour periodic variation was revealed in the four hour observation in June 2000, which makes ULX-3 one of the few that have periods. While the variation could be attributed to a brief outburst of an X-ray nova that was in its quiescence in June 2001, the X-ray nova picture is excluded

based on 20 years of observations with Einstein, ROSAT and Chandra observatories, because the source has been brighter than 10^{39} erg/sec for most of the time despite of the dramatic variations. If the two hour period is interpreted as the orbital period, the ULX is a LMXB system with a dwarf secondary of mass $\sim 0.3M_{\odot}$ filling its Roche Lobe and accreting mass onto the primary.

ULX-3 has been observed with HST/WFPC2 in filters F450W (B), F555W (V) and F814W (I). To register ULX-3 on the optical images, we utilize a nearby X-ray source, X12 in ObsID 1622, which is on the WF3 chip and far away from the spiral arm or any star forming regions. Two objects are found within the 3σ error circle of X12 on the optical images, one is a bright foreground star $1''.7$ away from the nominal Chandra position, another a faint object $0''.4$ away from the Chandra position with $B = 24.54$ mag, $V = 24.29$ mag, and $I = 24.04$ mag as calculated with HSTphot. With the extinction corrected for the Galactic HI column density of 1.6×10^{20} cm^{-2} , the faint object has $M_B = -5.00$ mag, $M_V = -5.23$ mag, and $M_I = -5.44$ mag. This is likely a field globular cluster given its isolated position and its red colors. The X-ray spectrum of X12 shows substantial flux above 1 KeV, with $F_X(1-2\text{KeV})/F_X(0.3-1\text{KeV}) = 0.29 \pm 0.15$. This is significantly harder than X-ray spectra of stars, for which there is essentially no emission above 1 KeV. Thus we identify the faint object as the optical counterpart for X12, which is presumably a LMXB system in the globular cluster, and register the ULX on the optical images based on this identification. The derived optical position for ULX-3, together with the X-ray and optical positions for X12, are listed in Table 3. The resulted error circle is of radius $\sim 0''.3$ (Figure 3).

ULX-3 falls on the rim of a young star cluster in the chain of star forming knots on the spiral arm of M51. The error circle is coincident with what appears to be a cavity between stars, with two faint objects within and a few on the edge. While the faint objects may not be the secondary of the ULX system which is a $\sim 0.3M_{\odot}$ dwarf and well below the detection limit, they, along with other stellar objects in the immediate vicinity of ULX-3, provide an age estimate for the system. The stellar objects within $0''.5$ of the corrected X-ray position are mostly red supergiants, as seen in the color-magnitude diagram for them and other stellar objects from the star cluster (Figure 4). The isochrones ($Z=0.020$) are overlaid on the diagram, and we found that these stellar objects span an age range of 10^7 – $10^{7.8}$ years. It is interesting to note that the brightest stars have left the main sequence, and all have ages above $\sim 10^7$ years, which may imply the star formation ended 10 million years ago.

ULX-5 have been observed in the second and third Chandra observations, with an average X-ray position R.A.=13h30m07.6s, Decl.=47d11m05.9s. Terashima & Wilson (2004) found that the spectra in both observations are better fitted with an absorbed power-law model (with $n_H \sim 1 \times 10^{21}$ cm^{-2}) than a multi-color disk model. The spectrum flattened

($\Gamma = 2.26$ to $\Gamma = 1.86$) and the luminosity dropped by 40% from 3.1×10^{39} erg/sec to 1.8×10^{39} erg/sec between the two observations. If the power-law spectra are analogous to the Low Hard state in Galactic black hole candidates and the state transition is governed by the mass accretion rate, the ULX would be emitting at less than a few percent of the Eddington luminosity, and a black hole of $>$ a few $\times 100M_{\odot}$ is required. If the power-law is from the Comptonization of thermal emission from the accretion disk with a high accretion rate and the ULX is emitting at 10% of the Eddington level as in the case of GRO J1655-40 (Kubota et al. 2001), the black hole may have a mass $\sim 120M_{\odot}$. However, it is unclear whether the power-law spectrum is operated by the above mechanisms, and whether the Eddington level of the ULX emission is valid for higher mass parallels for Galactic black hole candidates. Thus no concrete mass constraints can be placed on the primary of the ULX system from the X-ray spectra.

ULX-5 has been observed with HST/WFPC2 in filters F450W (B), F555W (V) and F814W (I). There is no other nearby X-ray sources that have optical counterparts on the WFPC2 images, so we overlay the X-ray position directly on the optical images as shown in Figure 5. The ULX is on a spiral arm, and within the $0''.8$ error circle are seven faint objects, the magnitudes of which are computed with HSTphot and listed in Table 4. The absolute M_V magnitudes of these candidates for the optical counterpart of ULX-5 have a range of $-4 \sim -5$ mag, and their $B - V$ colors range from -0.1 to 0.7 mag. As seen from the color-magnitude diagram (Figure 6), these candidates are evolved blue or red supergiants, and have an age range of $10^{7.4} - 10^{7.8}$ years. Similar to the stellar population around ULX-3, there seems to be a lack of bright stars younger than 10 million years in the vicinity of this ULX.

The positional accuracy of ULX-5 can be greatly improved with the help of a nearby X-ray source, X1 in ObsID 1622, that is $40''$ away from ULX-5. While this X-ray source appears to have an optical counterpart on a low spatial resolution optical image taken with the MDM 2.4m telescope, it is unfortunately not within the field of view of our HST observations. Future observations with HST/ACS can be designed to cover both X1 and ULX-5, and the relative positional accuracy can be improved to $\sim 0''.2$. Given the stellar density around ULX-5 (seven objects within the $0''.8$ error circle), such a small error circle would be able to identify one of the candidates as the unique optical counterpart for ULX-5, or none if the secondary is a low mass dwarf star below detection limits.

For the stellar populations around both ULXs, interestingly there seems to be a lack of very bright stars younger than 10 million years. It is unlikely for this lack to be a defect caused by the photometry package or the mis-calibration of the instruments, since such a lack is not present for the stellar population in NGC4559, for which we used the same instrument

and processed with the same procedures. It is difficult to diminish the lack by de-reddening the stars for the extinction, because by making the bright stars bluer and younger, the faint stars would be too blue to be predicted by the stellar models. The metal abundance of the star forming regions may affect our conclusion since stars with lower metallicity are bluer and brighter and have a shorter life. However, the lack of young bright stars persists if we change the metallicity, though lack of stars younger by slightly different ages. For example, if the metallicity is lower and $Z=0.001$, the stellar populations lack bright stars younger than 15 million years. If the metallicity is higher and $Z=0.100$, the stellar populations lack brighter stars younger than 6 million years. If the lack is real, it indicates that star formation spontaneously stopped 10 million years ago for some reasons. Alternatively, this could be a statistical defect due to small numbers of bright stars.

2.3. A ULX in NGC1313

NGC1313 is a barred Sd spiral galaxy with scattered star forming regions outside its D_{25} isophote at a distance of 3.7 Mpc (Tully 1988). Three bright X-ray point sources have been found in this galaxy, including SN1978K and two ULXs. Here we study one of the ULX, ULX-3 in Liu & Bregman (2005), which is $5'$ south of the galactic nucleus and in an isolated star forming region.

This ULX, along with SN1978K, has been observed many times with EINSTEIN, ROSAT, and recently Chandra and XMM. Zampieri et al. (2004) studied the long term variability of this ULX with all available observations, and found that this ULX is highly variable, and variability of up to a factor of 2 on a timescale of months is clearly present which is reminiscent of the behavior observed in Galactic X-ray binaries. The X-ray spectrum from an XMM observation in October 2000 has been studied and it is found to be better fitted with an absorbed multi-color disk plus a power-law model (Miller et al. 2003; Zampieri et al. 2004). The fit gives an HI column density of $3 \times 10^{21} \text{ cm}^{-2}$ and a color temperature of $\sim 150 \text{ eV}$, which if interpreted as the inner disk temperature implies an primary black hole of $M_{\bullet} \sim 10^3 M_{\odot}$.

Two Chandra observations are available in the archive, one observed in October 2002 (ObsID 2950, 20 kiloseconds), another in November 2002 (ObsID 3550, 15 kiloseconds). The average X-ray position is R.A.=03h18m22.27s, Decl.=−66d36m03.8s with an uncertainty of $0''.7$. The optical counterpart lies in a elongated bubble nebula with a diameter of $\sim 400 \text{ pc}$ (Pakull & Mirioni 2002), which shows an abrupt change in the absolute and relative intensity of the emission lines from east to west indicating variations in the physical conditions and/or geometry of the emission nebula (Zampieri et al 2004). By overlaying the X-ray position on

a Bessel R band image taken with the 3.6m telescope of ESO at La Silla in January 2002, Zampieri et al. (2004) found a faint object with $R = 21.6 \pm 0.2$ mag within the error circle. Such an identification was backed up by relative astrometry using nearby SN1978K.

We have observed the same region in the CTIO-I filter with IMACS mounted on the Magellan/Baade telescope. The observation has a better seeing ($\sim 0''.6$) than the 3.6m ESO image ($\sim 1''$), and is able to resolve the object B in the 3.6m ESO image into two objects B1 and B2 (Figure 7). The CTIO-I magnitudes were calculated with a 5-pixel aperture and calibrated with the photometric standards in the field L98, with a photometric calibration dispersion of 0.05 mag. The uncertainties in the magnitudes are estimated to be 0.2 mag. The CTIO-I magnitudes for the optical counterpart and nearby objects are listed in Table 5 in comparison to the R magnitudes from Zampieri et al. (2004).

The optical counterpart has $M_R = -6.2$ mag and $M_I = -4.5$ mag, both within the range of the absolute magnitudes for supergiants. It is a very interesting blue object in that $R-I_{CTIO} \approx -1.7$ mag, while the bluest stellar objects have $R-I \approx -0.32$ mag (Allen, 2000). It is even bluer after correcting for the extinction by the Galactic HI column density of $4 \times 10^{20} \text{ cm}^{-2}$ ($A_R = 0.179$ mag, $A_I = 0.130$ mag). If a maximum total HI column density of $3 \times 10^{21} \text{ cm}^{-2}$ is assumed, the correction is $A_R = 1.344$ mag and $A_I = 0.975$ mag. While the difference between the CTIO-I filter and Bessel I filter may lead to non-zero color terms, a color term of ~ 2 mag is not expected. This over-blueness of the counterpart may be attributable to non-thermal emission in the R band, e.g., extremely strong H_α emission line. This R-band excess may also be caused by dramatic variability between two observations in two years, or simply by errors in one of the measurements or both. We note the CTIO-I magnitude is not consistent with the R magnitude for object A, which is a G–M supergiant as seen from its low resolution spectrum (Zampieri et al. 2004) and should have $R-I \sim 0.5$ mag for a G8 supergiant or 1.1 mag for an M2 supergiant (Allen,2000). If the R-I color is corrected by ~ 1 mag, the optical counterpart would have $R-I \sim -0.7$ mag, bluer than the bluest stellar objects. Further observations with more filters including R and I are required to settle the problem.

2.4. A ULX in NGC628

NGC628 is a face-on Sc spiral galaxy with considerable grand design spiral structures at a distance of 9.7 Mpc (Tully 1988). This galaxy was observed in June 2001 (ObsID 2057, 46 kiloseconds) and in October 2001 (ObsID 2058, 46 kiloseconds) with the Chandra Observatory, and in February 2002 (ObsID 0154350101, 36.9 kiloseconds) and in January 2003 (ObsID 0154350201, 24.9 kiloseconds) with the XMM-Newton Observatory, which revealed a

ULX ~ 2.5 from the galactic nucleus, with an average X-ray position as R.A.=01h36m51.1s, Decl.=15d45m46.8s, on a chain of star forming knots that strays away from a main spiral arm.

This ULX showed quasi-periodic oscillations (QPO) with a quasi-period of 4,000-7,000 seconds (Liu et al. 2004). Its QPO is unique behavior among ULXs and Galactic X-ray binaries due to the combination of its burst-like peaks and deep troughs, its long quasi-periods, its high variation amplitudes of $> 90\%$, and its substantial variability between observations. The X-ray spectra in both Chandra observations are fitted by an absorbed accretion disk plus a power-law component, suggesting the ULX was in a spectral state analogous to the Low Hard state or the Very High state of Galactic black hole X-ray binaries. A black hole mass of $\sim 2-20 \times 10^3 M_{\odot}$ is estimated from the f_b-M_{\bullet} scaling relation found in the Galactic X-ray binaries and active galactic nuclei (Liu et al. 2004).

The ULX was observed in Bessel B, Bessel V, and CTIO-I filters with IMACS in search of its optical counterpart. A few X-ray sources have optical counterparts on the IMACS images, showing that the Chandra positions are accurate to better than $0''.6$ without systematic offsets. A direct overlay of the X-ray position on the optical images (Figure 9) reveals the ULX is surrounded by a blue shell structure, possibly a bubble nebula of ~ 300 pc as seen in the case of the ULX in NGC1313. An extended fuzzy object (C1) is marginally discernible at the nominal Chandra position, and could be a supergiant star that is the optical counterpart of the ULX. The counterpart could also be another brighter object (C2) which is $\sim 0''.4$ away from the nominal Chandra position.

The magnitudes for C1, C2, and three other objects within the 3σ error circle of the X-ray position of the ULX are listed in Table 6. The uncertainties are estimated to be as large as 0.4 mag owing to the crowdedness of the objects and the diffuse background. After the extinction is corrected for the Galactic HI column density of $\sim 5 \times 10^{20} \text{ cm}^{-2}$ ($A_B=0.352$ mag, $A_V=0.265$ mag, $A_I=0.163$ mag), the M_V magnitudes for these objects range from -7.3 mag to -9 mag, which is $\sim 0.7-3.4 \times 10^5$ times brighter than the Sun. The $B - V$ colors range from 0.03 mag to 0.23 mag, the same range for A0 - A8 stars. Given their extendedness, their absolute magnitudes and their colors, these objects are likely young star associations/clusters in the star forming region. However, any definite conclusions are premature given the large uncertainties in the magnitudes and colors, and the large seeing ($0''.6 \sim 30$ pc) for the ground-based observations. Further optical observations with HST are required to clarify the nature of these objects.

3. DISCUSSION

An essential step in understanding the nature of the enigmatic ULXs is to study them in other wavelengths, especially in optical. Along this line of thought, we have studied a sample of ULXs in optical with HST and the Magellan/Baade 6.4m telescope. These include the ULX in NGC3031, which is identified with an O8V star (Liu et al. 2002), and the ULX in NGC5204, which is identified with a B0Ib supergiant with considerable FUV emission from the accretion disk (Liu et al. 2004). Optical studies of five ULXs in four galaxies are reported in this paper. The ULX in NGC4559 is identified with an OB association in an isolated star forming complex on the outer edge of NGC4559. The ULX-3 in NGC5194 is located on the rim of a young star cluster on a spiral arm, and its probable secondary of $\sim 0.3M_{\odot}$ as inferred from its two hour period is below the detection limit. The ULX-5 in NGC5194 is located on a spiral arm, and identified with a few blue and red supergiants. The ULX in NGC1313 is identified to an object with R-I color bluer than the bluest stellar objects, indicative of non-thermal emission in the R band, or dramatic variability between two observations in two years, or errors in measurements. The ULX in NGC628 is located in a bubble nebula of ~ 300 pc on a chain of star forming knots, and identified with a few young stellar associations/clusters.

Optical studies have revealed a strong tendency for ULXs to occur in very young star forming regions, which suggests that ULXs are associated with the production and rapid evolution of short-lived massive stars. Pakull & Mirioni (2002) surveyed fifteen ULXs in eleven nearby galaxies with ground based telescopes, and found HII regions, (bubble) nebulae, and X-ray ionized nebulae (XIN) within the error circles of the ROSAT HRI positions for thirteen ULXs. Our optical studies of the ULXs show that their stellar environments are very young, for example, younger than $10^{7.6}$ years for the ULX in NGC3031, younger than $10^{7.6}$ years for the ULX in NGC4559, and younger than $10^{7.8}$ years for the two ULXs in NGC5194. These findings are consistent with the model that ULXs are HMXB systems undergoing thermal timescale mass transfer through Roche lobe overflow, which is a bright, short-lived, but common phase that must follow the familiar wind-fed phase of HMXBs, as is probably seen in SS433 (King et al. 2002).

The close connection between ULXs and HMXBs is dramatically demonstrated by the recent Chandra observation of the Cartwheel galaxy (Gao et al. 2003). The Chandra observation reveals more than 20 ULXs with $L_{0.5-10keV} \geq 3 \times 10^{39}$ erg/sec, most of which are confined in an expanding ring, the main site of recent massive star formation that started 3×10^8 years ago. The lack of radial spread of the ULXs suggests these ULXs must have ages $\leq 10^7$ years given the expansion velocity of the ring (Gao et al. 2003). King (2004) further points out that the initial secondary mass must be $\geq 15M_{\odot}$, and the total number

of HMXBs in the past 3×10^8 years is ≥ 3000 given the lifetime of these HMXBs ($\leq 10^7$ years), the beaming factor ($b \leq 0.1$), and the duty cycle ($d \sim 1$). If ULXs are IMBHs, the systems are likely to be transient with unstable accretion disks that probably have duty cycles $d \leq 10^{-2}$. It would be problematic to explain the observation with the IMBH model, since it is unlikely for this galaxy to produce the required $\geq 3 \times 10^4$ IMBHs to account for the observed ULXs.

Direct support for the HMXB scenario comes from the optical identifications of ULXs with massive stars as secondaries of the ULX systems. Only four ULXs have been identified with unique counterparts so far. A ULX in NGC3031 is identified with an O8 V star within the $0''.2$ error circle (Liu, Bregman, & Seitzer 2002). A ULX in NGC5204 is identified with a B0 Ib supergiant within the $0''.2$ error circle (Liu et al. 2004). A ULX in Holmberg II is identified with a point-like object within the $0''.6$ error circle, for which the absolute magnitude and B-V color are consistent with a range of spectral types from O4V to B3 Ib (Kaaret, Ward & Zezas 2004). A ULX in NGC1313 is identified with a point-like object within the $1''.4$ error circle, for which the absolute R magnitude is consistent with an early O star or an OB supergiant (Zamperi et al. 2004). Note that the optical identifications are usually based on positional coincidence, and may be nearby stars not related to the ULXs, especially in dense stellar fields with large error circles. The identification, therefore, is not secure until verified by other independent means. The identification for the ULX in NGC5204 is so far the only one verified by the spectroscopic observation with HST/STIS, which reveals, in addition to typical B0 Ib spectral features, an NV emission line suggestive of the existence of a hot accretion disk (Liu et al. 2004).

Once a ULX is identified with a stellar object as the secondary, follow-up spectroscopic observations of the secondary can determine its physical properties, its radial velocity curve and ultimately the mass of the primary. With medium/high resolution spectroscopy, one can identify spectral features and improve the spectral type estimated from the wide-band magnitudes and colors. In addition, possible spectral features from the accretion disk, e.g., the high ionization emission line of NV as in the case of NGC5204, can be used to secure the identification, or to elect the counterpart when more than one object are within the error circle as in the case of NGC4559. Once the mass (M_1) and size (R_1) of the secondary is determined empirically from its spectral type, the orbital properties will depend solely on the mass of the primary black hole (M_2) if the secondary is presumably filling its Roche lobe, for which the radius is $R_{cr} = \frac{0.49A}{0.6+q^{-2/3}\ln(1+q^{1/3})}$ (Eggleton 1983). Here A is the orbital separation, and $q = M_1/M_2$ is the mass ratio. With known M_1 and $R_{cr} = R_1$, one finds that the separation A , thus the orbital period P , depends only on the primary mass M_2 given the Kepler's Law $P^2/A^3 = 4\pi^2G(M_1 + M_2)$. The rotational velocity of the secondary also depends on the primary, with $v_1^2 = GM_2^2(M_1 + M_2)/A$.

The expected periods and rotational velocities are calculated as a function of the primary mass for a secondary of B0 Ib supergiant with $M_1 = 25M_\odot$ and $R_1 = 30R_\odot$ as an example (Figure 10). For the primary mass increases from $3 M_\odot$ to $10^3 M_\odot$, the orbital period increases from ~ 200 hours to ~ 300 hours at $100M_\odot$ then decreases to ~ 280 hours, while the rotational velocity of the secondary increases monotonically from 30 km/sec to 10^3 km/sec. Doppler shifts of such rotational velocities are easy to detect as they in a edge-on viewing geometry lead to a line shift of $0.45(\lambda/4500\text{\AA})$ for a $3 M_\odot$ black hole, $1.5 (\lambda/4500\text{\AA})$ for a $100 M_\odot$ black hole, and $15 (\lambda/4500\text{\AA})$ for a $10^3 M_\odot$ black hole. By taking a series of spectroscopic observations and constructing a radial velocity curve of the secondary, we would be able to determine the mass of the primary black hole, or the lower limit of the mass if the ULX system is not viewed edge-on.

Optical studies have also revealed a few ULXs with low mass secondaries. These include a ULX in NGC4565 (Wu et al. 2001) and two ULXs in the elliptical galaxy NGC1399 (Angelini et al. 2001) identified with globular clusters. The secondaries in these ULXs must be low mass stars owing to lack of massive stars in globular clusters. Another example is the ULX-3 in NGC5194, for which the secondary mass is estimated to be $\sim 0.3M_\odot$ if the observed two hour period is its orbital period, and if the secondary is overflowing the Roche lobe. The estimated secondary mass will be lower if the secondary is not filling its Roche lobe. Note that it is not necessary for the secondary to fill the Roche lobe to get high luminosities. King (2002) suggests that high inflow rates can be obtained in the outburst phase of soft X-ray transients (e.g., GRS 1915+105), which exists for most LMXBs, and inevitable for any LMXB with orbital period ≥ 2 days. For example, the inflow rate will exceed $\sim 10^{-7}M_\odot/yr$ for a $10M_\odot$ black hole if the orbital period ≥ 1 day, and lead to a total luminosity of $\geq 10^{39}$ erg/sec. The outburst phase is long and may span decades, but the quiescent intervals are much longer, and the duty cycle is $\ll 1$, which decreases with increasing orbital periods (King 2002).

We would like to thank Renato Dupke, Eric Miller for helpful discussions. We gratefully acknowledge support for this work from NASA under grants HST-GO-09073.

REFERENCES

- Abramowicz, M., Kluzniak, W., McClintock, J., and Remillard, R, 2004, ApJL, 609, L63
- Aldcroft, T.L., Karovska, M., Cresitello-Dittmar, M.L., Cameron, R.A., and Markevitch, M.L., 2000, Proc. SPIE, 4012, 650

- Allen's Astrophysical quantities, fourth edition, 2000
- Angelini, L., Loewenstein, M., and Mushotzky, F., 2001, ApJ, 557, L35
- Begelman, M.C., 2002, ApJ, 568, L97
- Belloni, T., and Hasinger, G., 1990, A&A, 227, L33
- Bohlin, R., Savage, B. D. & Drake, J. F., 1978, ApJ, 224, 132
- Colbert, E. J. M. and Mushotzky, R. F. 1999, ApJ, 519, 89
- Colbert, E. and Ptak, A. 2002, ApJS, 143,25
- Cropper, M., Soria, R., Mushotzky, R., Wu, K., Markwardt, C., and Pakull, M., 2004, MNRAS, 349, 39
- Dolphin, A.E., 2000, PASP, 112, 1383
- Eggleton, P.P., 1983, ApJ, 268, 368
- Fabbiano, G. 1989, ARA&A, 27, 87
- Gao, Y., Wang, Q., Appleton, P., and Lucas, R., 2003, ApJL, 596, 171
- Georganopoulos, M., Aharonian, F.A., and Kirk, J.G., 2002, A&A, 388, L25
- Kilgard, R., Kaaret, P., Krauss, M., Prestwich, A., Raley, M., and Zezas, A., 2002, ApJ, 573, 138
- Lejeune, T. and Schaerer, D., 2001, A&A 366, 538
- Liu, J., Bregman, J., and Seitzer, P., 2002, ApJL, 580, 31
- Liu, J., Bregman, J., and Irwin, J., 2002, ApJL, 581, 93
- Liu, J., Bregman, J., Irwin, J., and Seitzer, P., 2004, ApJ, 602, 249
- Liu, J., and Bregman, J., 2005, ApJS, in press
- Liu, J., Bregman, J., Lloyd-Davies, E., Irwin, J., Espaillat, C., and Seitzer, P., 2004, submitted
- King, A.R., Davies, M.B., Ward, M.J., Fabbiano, G., and Elvis, M. 2001, ApJ, 552, L109
- King, A.R., 2002, MNRAS, 335, 513

- King, A.R., 2004, MNRAS, 347, L18
- Kubota, A., Makishima, K., and Ebisawa, K., 2001, ApJ, 560, L147
- Makishima, K., Kubota, A., Muzuno, T., Ohnishi, T., Tashiro, M., et al. 2000, ApJ, 535, 632
- Miller, J., Fabbiano, G., Miller, M., and Fabian, A., 2003, ApJ, 585, 37
- Pakull, M.W. and Mirioni, L., 2002, astro-ph/0202488
- Kaaret, P., Ward, M., and Zezas, A., 2004, MNRAS, 351, L83
- Portegies Zwart, S., and McMillan, S., 2002, ApJ, 576, 899
- Schmidt-Kaler, Th., 1982, *Landolt-Bornstein: Numerical Data and Functional Relationships in Science and Technology*, eds. Schaifers, K. and Voigt, H.H., VI/2b, P.15-31
- Soria, R., Cropper, M., Pakull, M., Mushotzky, R., and Wu, K., 2004, MNRAS, 356, 12
- Strohmayer, T., and Mushotzky, R., 2003, ApJL, 586, 61L
- Swartz, D., Ghosh, K., Tennant, A., and Wu, K., 2004, ApJS, 154, 519
- Terashima, Y., and Wilson, A., 2004, ApJ, 601, 735
- Tully, R.B., 1988, *Nearby galaxies catalog*
- Tully, R.B., Shaya, E.J., Pierce, M.J., 1992, ApJS, 80, 479
- Wu, H., Xue, S.J., Xia, X.Y., Deng, Z.G., and Mao, S.D. 2002, ApJ, 576, 738
- Zampieri, L., Mucciarelli, P. et al., 2004, ApJ, 603, 523

Table 1. The optical position for the ULX in NGC4559

Object	ACIS-S3				WFPC2				
	RA	DEC	RA_ERR (arcsec)	DEC_ERR (arcsec)	Chip	X (pix)	Y (pix)	RA	DEC
X4	12:35:48.56	27:55:31.5	0.07	0.17	2	584.0	237.0	12:35:48.64	27:55:32.0
ULX	12:35:51.71	27:56:04.1	0.01	0.01	1	445.7	430.7	12:35:51.79	27:56:04.6
X5	12:35:47.67	27:56:57.2	0.12	0.14	3	584.0	237.0	12:35:47.76	27:56:56.4
ULX	12:35:51.70	27:56:04.9	0.03	0.03	1	445.7	430.7	12:35:51.79	27:56:04.1

Table 2. Optical counterpart Candidates for NGC4559-ULX

Candidate	m_B	app. mag.	m_I	M_B	5.8 Mpc		9.7 Mpc		
		m_V			M_V	M_I	M_B	M_V	M_I
C-1	24.82±0.083	24.56±0.048	24.08±0.076	-3.894	-4.177	-4.69	-5.004	-5.287	-5.8
C-2	25.18±0.117	24.24±0.041	23.1±0.031	-3.529	-4.499	-5.667	-4.639	-5.609	-6.777
C-3	24.46±0.137	23.91±0.078	22.95±0.057	-4.258	-4.831	-5.817	-5.368	-5.941	-6.927
C-4	22.79±0.022	23±0.016	23.2±0.04	-5.927	-5.738	-5.575	-7.037	-6.848	-6.685

Table 3. The optical position for ULX-3 in NGC 5194

Object	ACIS-S3				WFPC2				
	RA	DEC	RA_ERR (arcsec)	DEC_ERR (arcsec)	Chip	X (pix)	Y (pix)	RA	DEC
X12	13:29:56.25	47:14:51.5	0.09	0.08	3	304.0	604.0	13:29:56.21	47:14:51.5
ULX	13:30:01.01	47:13:44.0	0.15	0.12	1	392.5	400.1	13:30:00.97	47:13:44.0

Table 4. Optical Counterpart candidates for ULX-5 in NGC 5194

candidate	m_B	m_V	m_I
	mag	mag	mag
c1	25.788±0.229	25.562±0.093	25.079±0.192
c2	25.751±0.163
c3	...	26.052±0.222	24.946±0.174
c4	24.409±0.057	24.493±0.041	24.327±0.085
c5	25.803±0.242	25.142±0.128	23.033±0.038
c6	24.875±0.1	24.26±0.036	23.69±0.05
c7	25.357±0.138	25.376±0.086	...

Table 5. Optical counterpart to NGC1313-ULX and nearby objects

object	I_{CTIO} mag	m_R mag	M_I mag	M_R mag
A	19.8	19.8	-8.04	-8.04
B1	22.8		-5.04	
B2	22.9		-4.94	
B1+B2	22.1	20.7	-5.74	-7.14
C(ULX)	23.3	21.6	-4.54	-6.24
D	17.1	17.8	-10.74	-10.04

Table 6. Optical Counterpart candidates for the ULX in NGC628

Candidate	m_B mag	m_V mag	I_{CTIO} mag	M_B mag	M_V mag	M_I mag
C1	22.91	22.79	22.04	-7.02	-7.14	-7.89
C2	21.87	21.71	21.47	-8.06	-8.22	-8.46
C3	22.65	22.43	21.89	-7.28	-7.496	-8.04
C4	22.53	22.22	21.82	-7.401	-7.712	-8.11
C5	21.39	21.28	20.98	-8.541	-8.652	-8.95

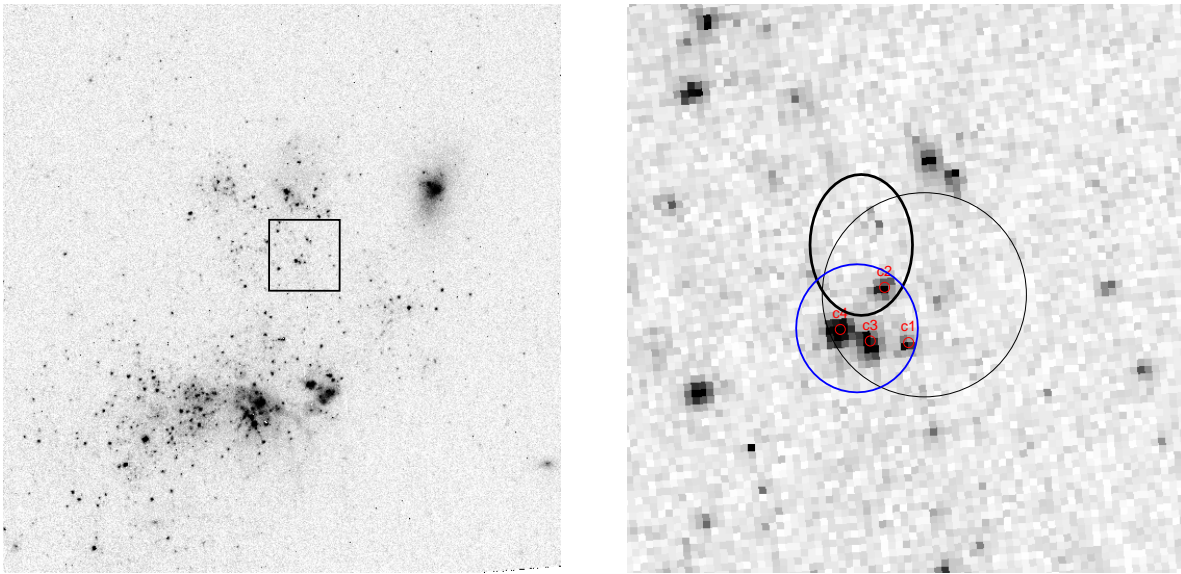


Fig. 1.— The optical identification of the ULX in NGC4559. The ULX, enclosed by a box region of $80 \text{ PC pixels} \times 80 \text{ PC pixels}$ in the left panel, lies between two young star clusters on a F555W PC image. A zoom-in of the boxed region is shown in the right panel. The $0''.6$ thin error circle (thin) was adopted by Cropper et al., the thick round error circle was based on the identification of X5 as a point source, and the error ellipse was based on the identification of X4 as an extended source. North is up for all images in this paper.

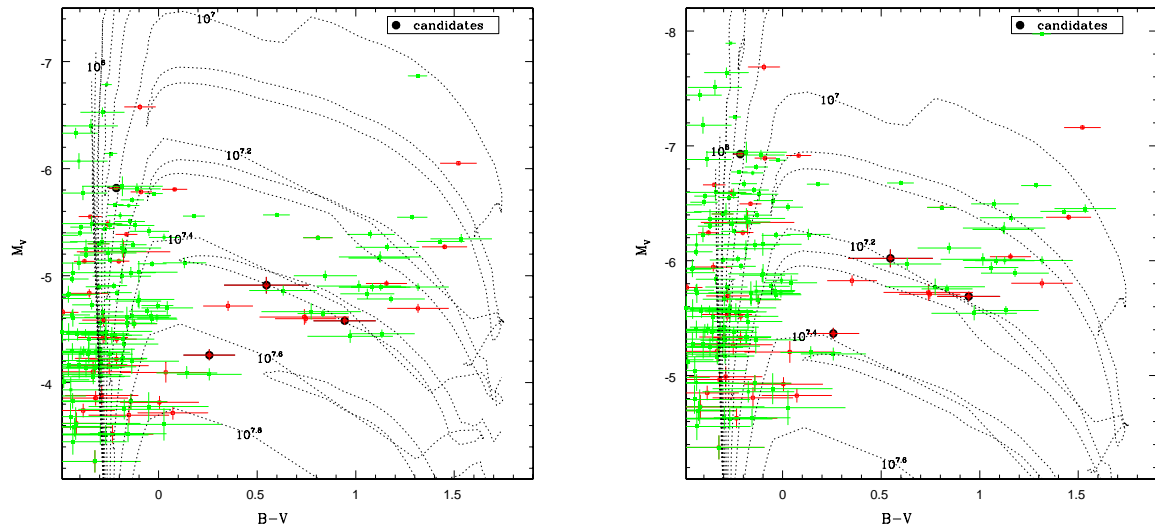


Fig. 2.— The color-magnitude diagrams for the four optical counterpart candidates for the ULX in NGC4559 and the nearby stars. The distance to NGC4559 is taken as 5.8 Mpc for the left panel, and 9.7 Mpc for the right panel. In both diagrams the isochrones from Lejeune & Schaerer 2001 with $Z=0.020$ are overplotted for comparison.

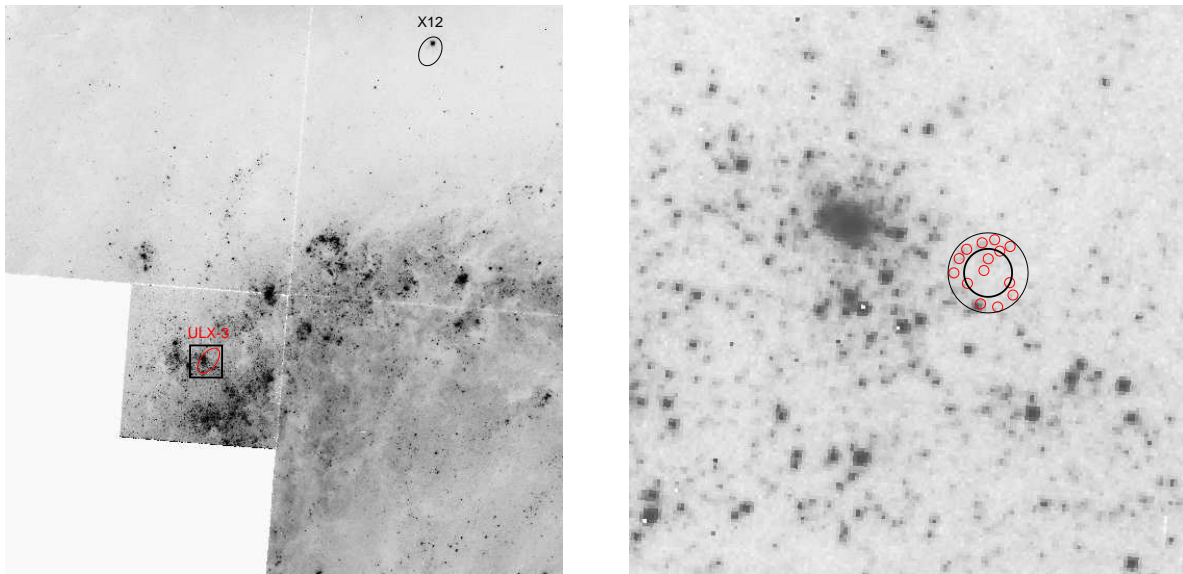


Fig. 3.— The optical identification of the ULX-3 in NGC5194. In the left panel, the 3σ error ellipses of the X-ray positions of ULX-3 and X12 are overlaid on a mosaic WFPC2 image. The ULX position was adjusted by identifying X12 to a possible globular cluster as described in the text. A zoom-in of the boxed region ($80 \text{ PC pixels} \times 80 \text{ PC pixels}$) is shown in the right panel. The thick circle around the adjusted ULX position has a radius of $0''.3$, and the thin circle has $0''.5$.

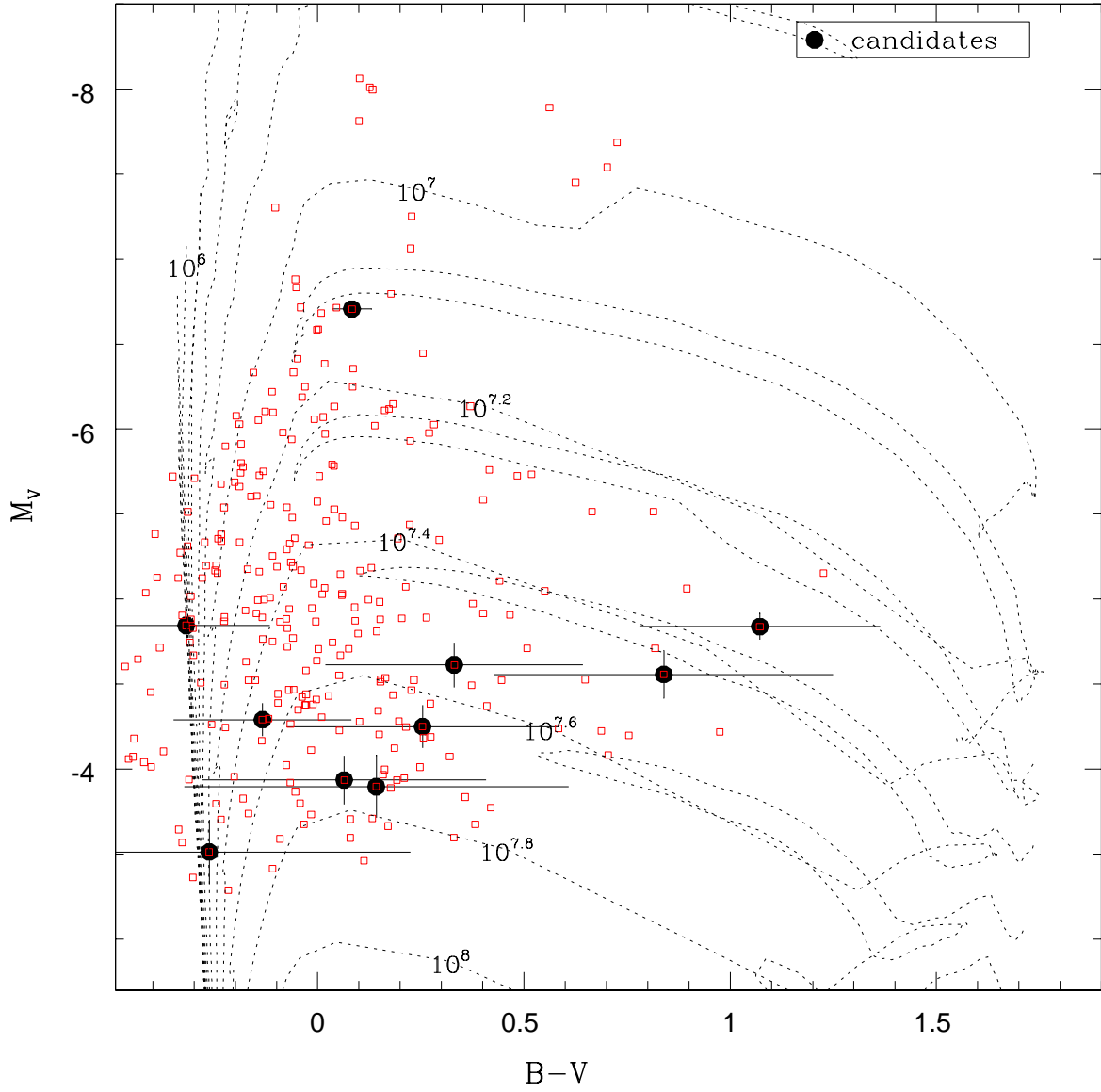


Fig. 4.— The color-magnitude diagram for the nearby stars around the ULX-3 in NGC5194. The filled circles are those within $0''.5$ of the adjusted ULX position. The isochrones from Lejeune & Schaerer 2001 with $Z=0.020$ are overplotted for comparison.

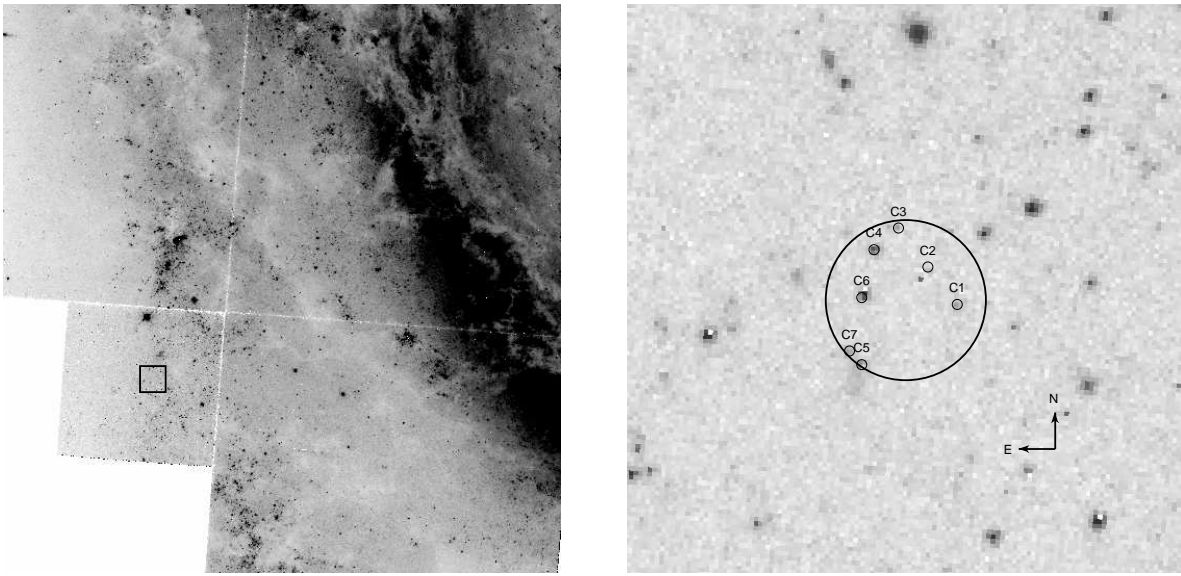


Fig. 5.— The optical identification of the ULX-5 in NGC5194. The ULX-5, enclosed in a boxed region of 80 pixels \times 80 pixels, is on the outer edge of a spiral arm as seen from the mosaic WFPC2 image in the left panel. A zoom-in of the boxed region is shown in the right panel. Seven point sources are enclosed in the $0''.8$ error circle around the nominal X-ray position.

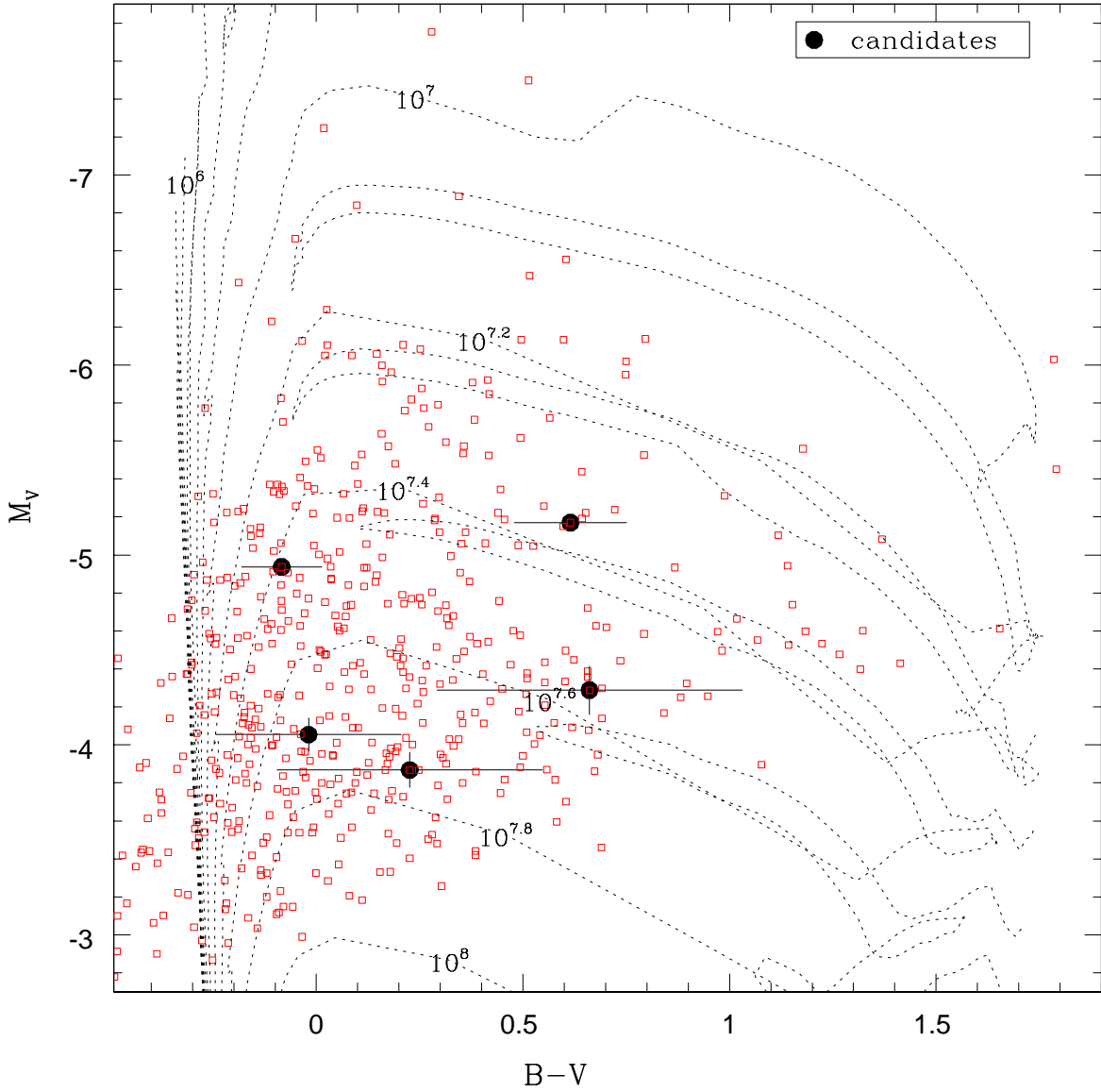


Fig. 6.— The color-magnitude diagram for the nearby stars around the ULX-5 in NGC5194. The filled circles are those within the $0.8''$ error circle of the nominal ULX position. The isochrones from Lejeune & Schaerer 2001 with $Z=0.020$ are overplotted for comparison.

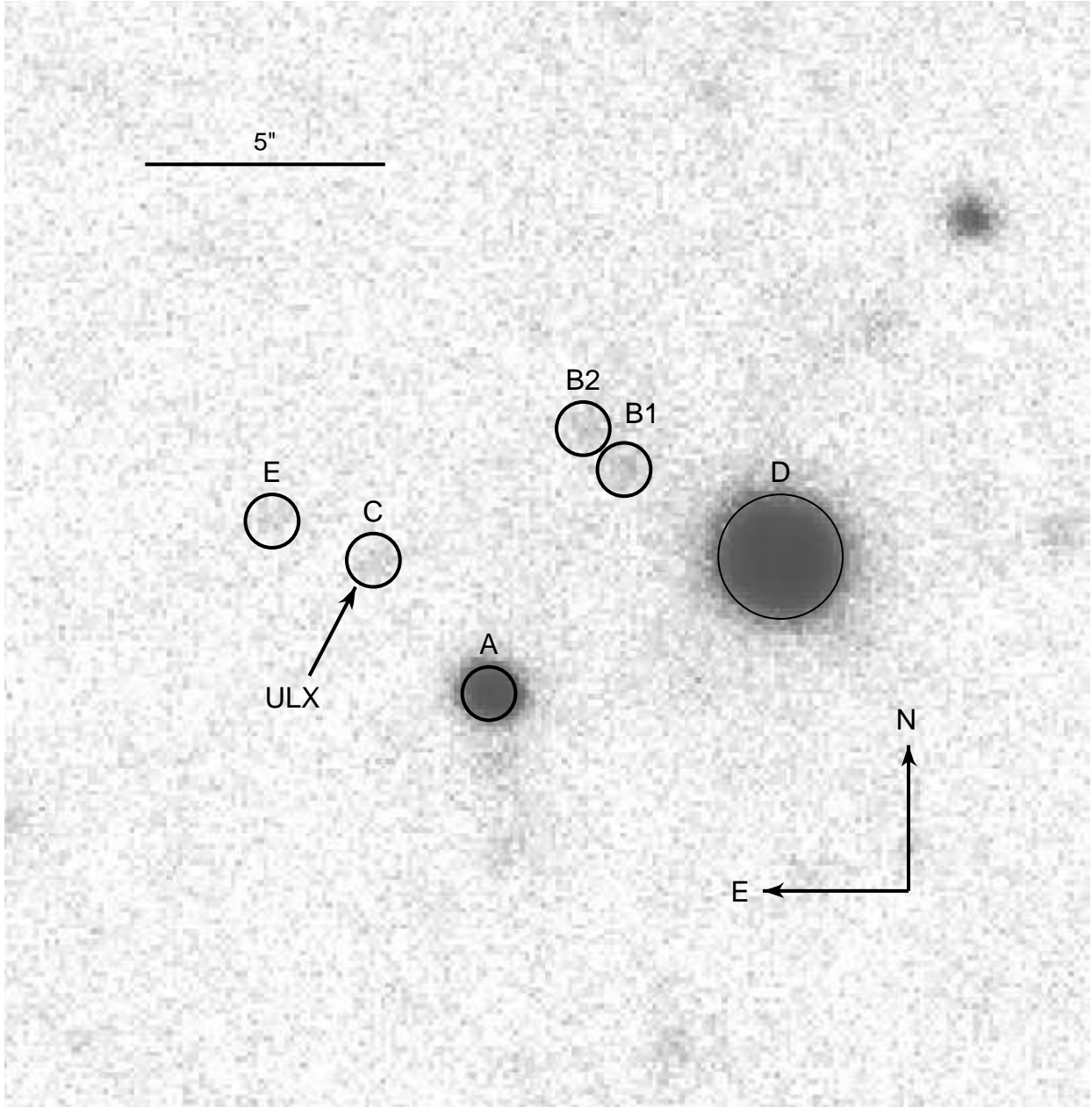


Fig. 7.— The optical counterpart for the ULX in NGC1313 on a CTIO-I image taken with the 6.4 meter Magellan/Baade telescope. The object names follow those in Zampieri et al. (2004), except that the object B on their R image taken with the 3.6 meter ESO telescope is resolved into two objects.

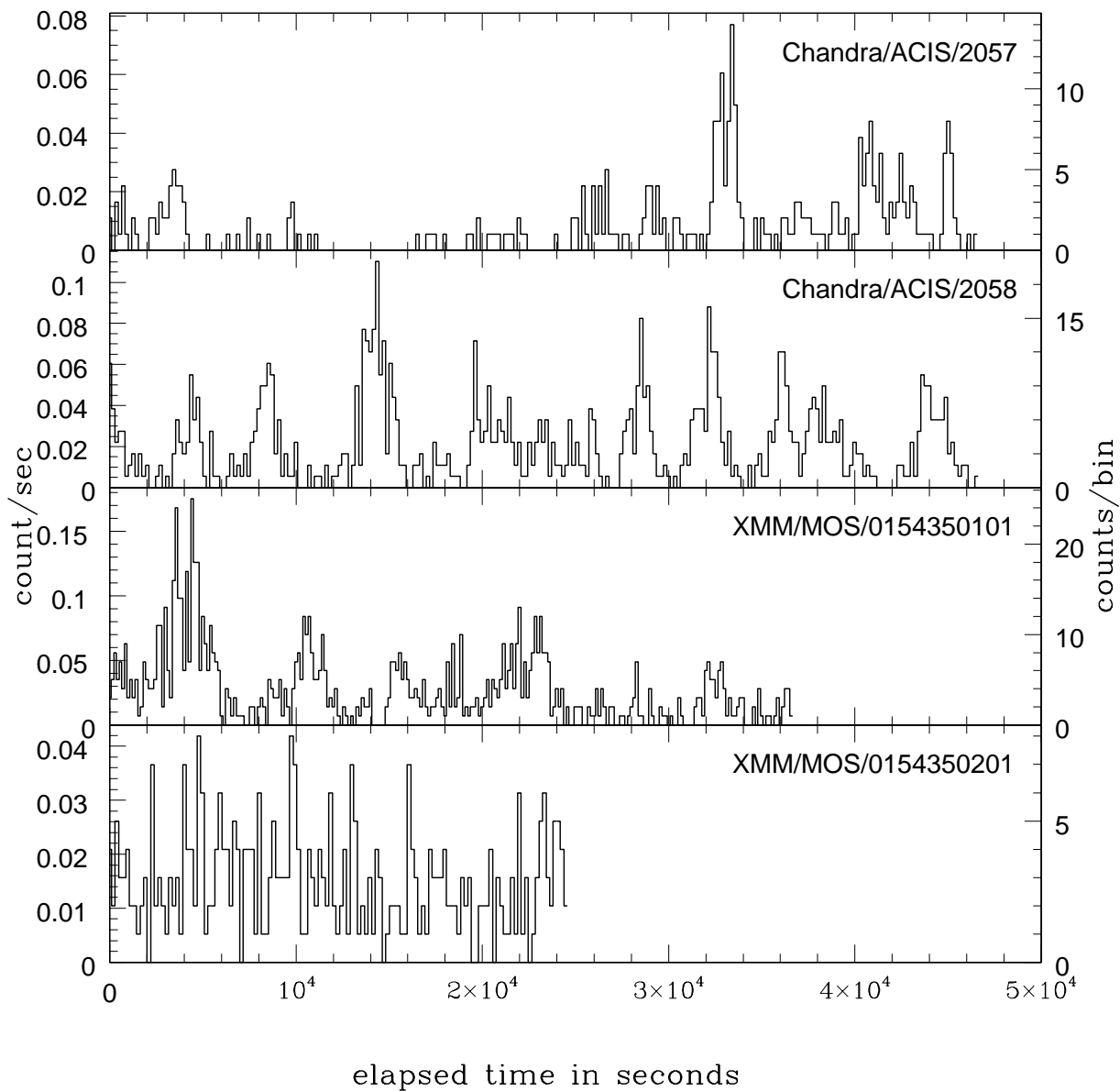


Fig. 8.— The light curves for the ULX in NGC628 in four observations. The quasi-periodic oscillations are apparent from the light curves, and unique for its burst-like peaks and deep troughs, its long quasi-period of ~ 4 – 7 kiloseconds, its high variation amplitudes, and its substantial variability between observations. Overplotted for comparison are sinusoidal curves with the periods of 4000/4000/7000/6000 seconds respectively. For details see Liu et al. (2004).

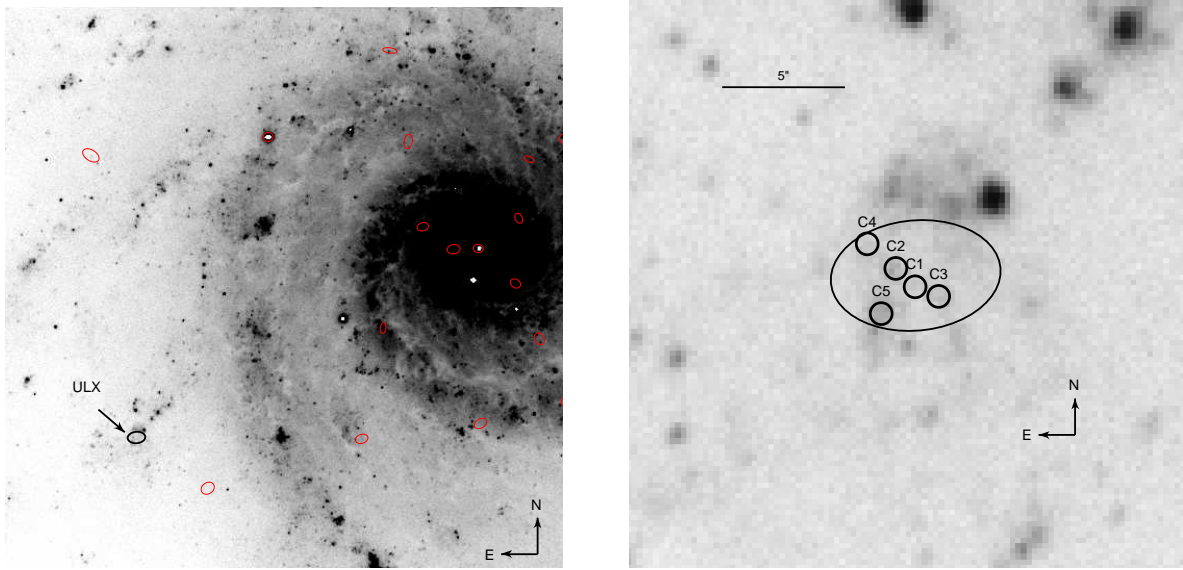


Fig. 9.— The optical identification of the ULX in NGC628. The left panel is a V image taken with the 6.4 meter Magellan/Baade telescope. Overlaid on the image are the 3σ error ellipses for the X-ray positions calculated with WAVDETECT. The ULX is on a chain of star forming knots that strays away from a main spiral arm. The right panel shows the immediate environments of the ULX.

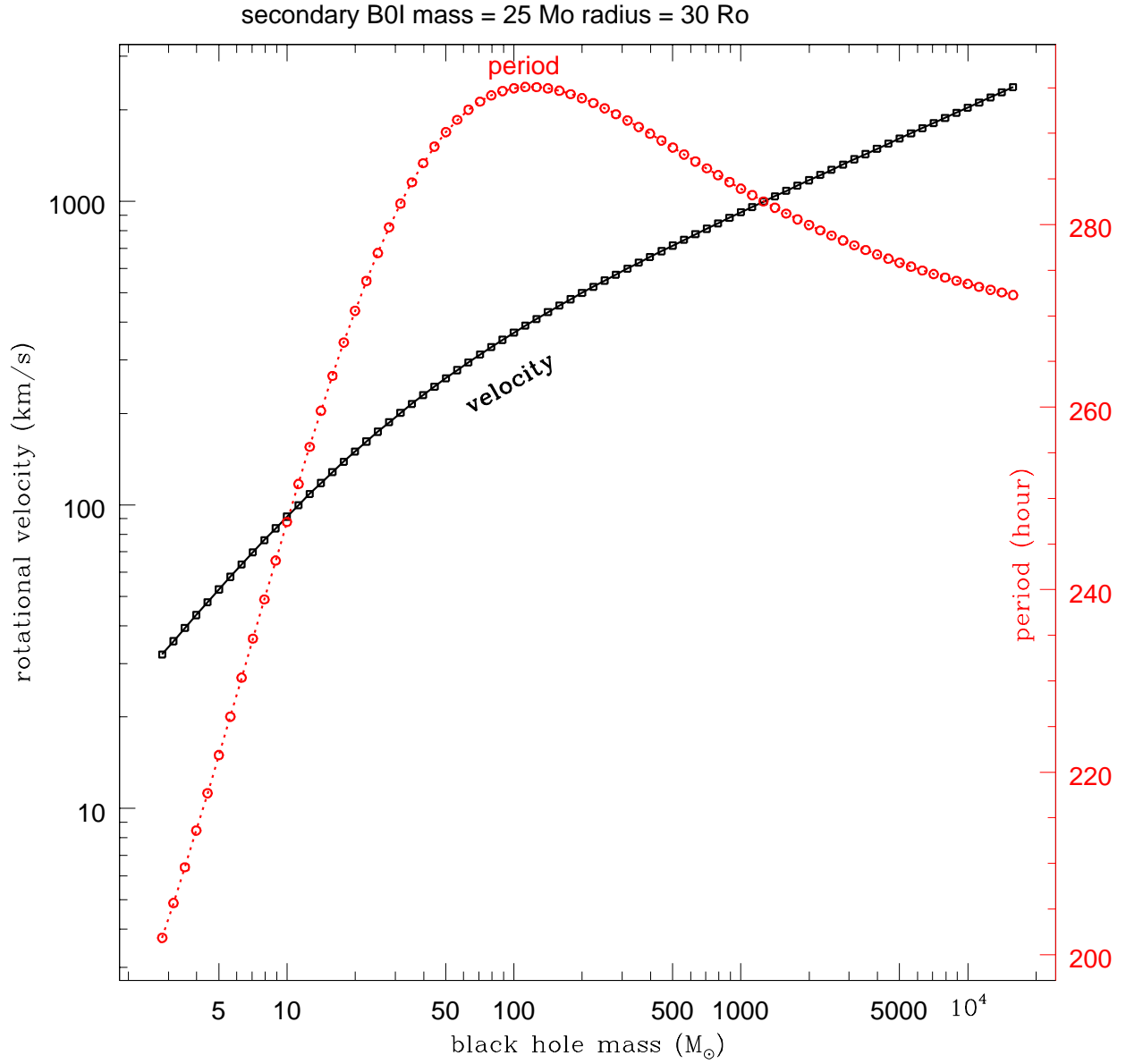
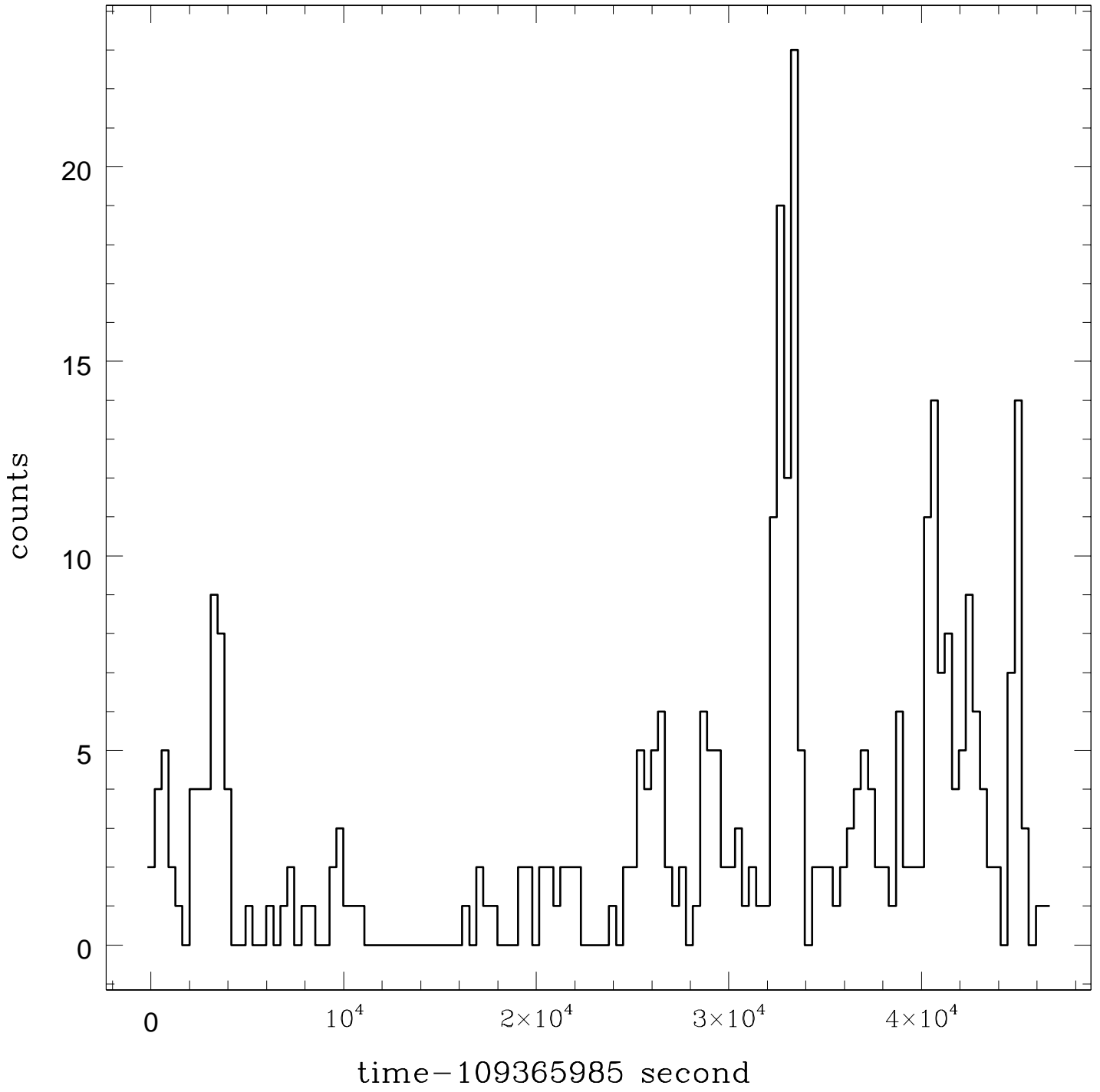


Fig. 10.— The expected orbital period and rotational velocity for a binary system with a B0 Ib secondary ($R = 30R_{\odot}, M = 25M_{\odot}$) filling its Roche lobe.

ulx2057bin128lc.ps



ulx2058bin128lc.ps

